

Atmospheric Parameters of 169 F, G, K and M-type Stars in the *Kepler* Field*

J. Molenda-Żakowicz¹, S.G. Sousa², A. Frasca³, K. Uytterhoeven^{4,5}, M. Briquet^{6,7}, H. Van Winckel⁷, D. Drobek¹, E. Niemczura¹, P. Lampens⁸, J. Lykke⁹, S. Bloemen⁷, J.F. Gameiro^{2,10}, C. Jean⁷, D. Volpi⁸, N. Gorlova⁷, A. Mortier^{2,10}, M. Tsantaki^{2,10}, G. Raskin⁷

¹ *Instytut Astronomiczny Uniwersytetu Wrocławskiego, ul. Kopernika 11, 51-622 Wrocław, Poland, E-mail: molenda@astro.uni.wroc.pl*

² *Centro de Astrofísica, Universidade do Porto, Rua das Estrelas, 4150-762 Porto, Portugal*

³ *INAF, Osservatorio Astrofisico di Catania, via S. Sofia, 78, 95123 Catania, Italy*

⁴ *Instituto de Astrofísica de Canarias, 38200 La Laguna, Tenerife, Spain*

⁵ *Departamento de Astrofísica, Universidad de La Laguna, 28206 La Laguna, Tenerife, Spain*

⁶ *Institut d'Astrophysique et de Géophysique, Université de Liège, Allée du 6 Août 17, Bât B5c, 4000 Liège, Belgium*

⁷ *Instituut voor Sterrenkunde, KU Leuven, Celestijnenlaan 200D, 3001 Leuven, Belgium*

⁸ *Koninklijke Sterrenwacht van België, Ringlaan 3, 1180 Brussel, Belgium*

⁹ *Nordic Optical Telescope, 38700 Santa Cruz de La Palma, Spain*

¹⁰ *Departamento de Física e Astronomia, Faculdade de Ciências, Universidade do Porto, Portugal*

Accepted 1988 December 15. Received 1988 December 14; in original form 1988 October 11

ABSTRACT

The asteroseismic and planetary studies, like all research related to stars, need precise and accurate stellar atmospheric parameters as input. We aim at deriving the effective temperature (T_{eff}), the surface gravity ($\log g$), the metallicity ($[\text{Fe}/\text{H}]$), the projected rotational velocity ($v \sin i$) and the MK type for 169 F, G, K, and M-type *Kepler* targets which were observed spectroscopically from the ground with five different instruments. We use two different spectroscopic methods to analyse 189 high-resolution, high-signal-to-noise spectra acquired for the 169 stars. For 67 stars, the spectroscopic atmospheric parameters are derived for the first time. KIC 9693187 and 11179629 are discovered to be double-lined spectroscopic binary systems. The results obtained for those stars for which independent determinations of the atmospheric parameters are available in the literature are used for a comparative analysis. As a result, we show that for solar-type stars the accuracy of present determinations of atmospheric parameters is ± 150 K in T_{eff} , ± 0.15 dex in $[\text{Fe}/\text{H}]$, and ± 0.3 dex in $\log g$. Finally, we confirm that the curve-of-growth analysis and the method of spectral synthesis yield systematically different atmospheric parameters when they are applied to stars hotter than 6,000 K.

Key words: stars: atmospheric parameters – open clusters and associations: individual: NGC 6811, NGC 6819 – space missions: *Kepler*

* Based on observations acquired at the Canada-France-Hawaii Telescope (CFHT) which is operated by the National Research Council of Canada, the Institut National des Sciences de l'Univers of the Centre National de la Recherche Scientifique of France, and the University of Hawaii, the Telescope Bernard Lyot (USR5026) operated by the Observatoire Midi-Pyrénées (Université de Toulouse and the Institut National des Science de l'Univers of the Centre National de la Recherche Scientifique of France), the Nordic Optical Telescope, operated jointly by Denmark, Finland, Iceland, Norway, and Sweden, and with the Mercator telescope,

operated by the Flemish Community, both located on the island of La Palma at the Spanish Observatorio del Roque de los Muchachos of the Instituto de Astrofísica de Canarias, and the M.G. Fracastoro station of the INAF - Osservatorio Astrofisico di Catania, Italy. The Mercator observations were obtained with the HERMES spectrograph, which is supported by the Fund for Scientific Research of Flanders (FWO), Belgium, the Research Council of K.U.Leuven, Belgium, the Fonds National de la Recherche Scientifique (FNRS), Belgium, the Royal Observatory of Belgium,

1 INTRODUCTION

Since March 2009, the 105 deg² field located in between the constellations of Cygnus and Lyra has been continuously monitored by the NASA space mission *Kepler* (Borucki et al. 2003; Koch et al. 2010). The effective temperature (T_{eff}), surface gravity ($\log g$), and metallicity ([Fe/H]) of stars in the *Kepler* field were derived from the Sloan *griz* photometry and are provided in the *Kepler* Input Catalog (KIC, Brown et al. 2011). KIC was created with the aim of providing a distinction between main-sequence stars and giants in the temperature range from 4,500 to 6,500 K. Within that range, the nominal precision of the values of T_{eff} and $\log g$ in KIC is 200 K and 0.5 dex, respectively. For hotter and cooler stars, the values of T_{eff} and $\log g$ in KIC become imprecise, while the estimates of [Fe/H] are poor in general (Brown et al. 2011).

This situation is very unfortunate for asteroseismic and planetary studies which require precise and accurate atmospheric parameters of stars to produce reliable results (see, e.g., Stello et al. 2009; Creevey et al. 2012). Therefore, ground-based follow-up observations aiming at deriving the values of T_{eff} , $\log g$, and [Fe/H] are essential for further investigation of the *Kepler* targets. Such programmes started well before the *Kepler* satellite was launched (see Molenda-Żakowicz et al. 2007) and then, after the successful launch of the mission, were continued in the framework of the *Kepler* Asteroseismic Science Consortium¹ (KASC) as a series of coordinated observing programmes for systematic spectroscopic and photometric observations (see Uytterhoeven et al. 2010a,b).

The first results of those proposals have been published by Molenda-Żakowicz et al. (2010, 2011); Frasca et al. (2011); Fröhlich et al. (2012); Bruntt et al. (2012); Thygesen et al. (2012). In this paper, we report the results of spectroscopic analysis of a next subset of F, G, K, and M-type stars. In Sect. 2, we outline the method of selecting targets. In Sect. 3, we provide information about the instruments and data acquisition, reduction and calibration. Our methods of analysis are described in Sect. 4. In Sect. 5, the atmospheric parameters are provided and compared with other determinations reported in the literature. Sect. 6 contains a discussion of the accuracy of our results and the accuracy of the determinations of the atmospheric parameters of the solar-type stars in general. Sect. 7 provides a summary.

2 TARGET SELECTION

Targets for each instrument were selected slightly differently. Those selected for the FIES spectrograph at the Nordic Optical Telescope (the principal investigator: KU) and the HERMES spectrograph at the Mercator telescope (the principal investigator: MB and EN) included solar-like p-mode oscillators, γ Dor, δ Sct, and β Cep-type stars, and stars in the open clusters NGC 6811 and NGC 6819 requested for observations by the KASC community. In this paper, we

analyse the F, G, K, and M-type stars observed with FIES (ten stars) and HERMES (twenty stars). The results obtained for early-type stars will be presented by Niemczura et al. and Catanzaro et al. (in prep.) When prioritising targets in those two proposals, more weight was given to stars that showed a particular interesting variable signal in the *Kepler* light-curves and hence promise to be the best targets for a comprehensive asteroseismic study, and to stars that were of interest to different KASC working groups. Brightness of the stars was another important selection factor. Since we made use of medium- and high-resolution spectrographs at 1-m and 3-m-class telescopes, we were limited to stars brighter than about $V = 13$ mag. The final list of targets observed with HERMES included stars falling into the magnitude range of $10 > V > 8$ mag, while those observed with FIES, into the range of $11.5 > V > 7$ mag.

The 18 stars which were observed with the FRESCO spectrograph at the 91-cm telescope at INAF-Osservatorio Astrofisico di Catania (INAF-OACt, the principal investigator: JM-Ż) were selected from faint ($11 > V > 8$ mag), late-type ($1.7 > B - V > 0.5$ mag), close (the parallax $\pi > 20$ mas) stars in the Tycho catalogue (Høg et al. 2000) which are optical counterparts of X-ray sources in the ROSAT All-Sky Survey Catalogue (see Guillout et al. 1999). These stars were proposed for *Kepler* asteroseismic targets and for the follow-up ground-based observations by AF in the first call for proposals announced by KASC.

Our list of programme stars includes also 91 *Kepler* targets which were observed with the ESPaDOnS spectrograph at the Canada-France-Hawaii Telescope (the principal investigator: Claude Catala) and 50 stars observed with the NARVAL spectrograph at the Bernard Lyot Telescope (the principal investigators: KU and Claude Catala), for which the data are now public². Those two instruments observed solar-type stars with the widest range of brightness: $12 > V > 7$ mag.

The total number of spectra which we analyse is 189. However, because 15 stars were observed with two instruments and one star, with three, the number of the individual stars that we discuss in this paper is 172. Three of those stars are double-lined spectroscopic binaries (SB2) and therefore, we do not compute their atmospheric parameters; those values are provided for 169 stars. The stars with multiple observations are used for an internal check of the consistency of our results. Those for which T_{eff} , $\log g$, and [Fe/H] have been derived by Bruntt et al. (2012) or Thygesen et al. (2012) from the ESPaDOnS and NARVAL spectra are included for the sake of analysing possible differences in the results obtained by means of different methods.

124 stars from our sample have been recently discovered to show solar-like oscillations and eleven, to show other types of photometric variability (see Table 3 and the references therein.) Four stars fall into the field of the open cluster NGC 6811 (KIC 9655101, 9655167, 9716090, and 9716522) and three, into the field of NGC 6819 (KIC 5024851, 5112786, and 5199859.) KIC 3632418 (= Kepler 21b) is a planet-hosting star (Howell et al. 2012) while KIC 8866102,

9414417, 9955598, and 10963065 are *Kepler* candidates for stars with planets³.

3 OBSERVATIONS

Our programme stars were observed with five different instruments. In Table 1, we provide names of those instruments, the names of the telescopes, the acronyms of the observatories, the number of acquired spectra (n), the year in which the data were acquired, the spectral range and the resolving power (R) of the spectrograph, the exposure time, and the typical signal-to-noise ratio (S/N) along with the location in the wavelength where it was measured.

For all the instruments, the bias, flat field, and calibration lamp measurements were acquired in the evening and the morning. For FIES, additional spectra of the calibration lamp were obtained before each science observation. The data were reduced and calibrated following standard reduction procedures which included subtraction of the bias frame, correction for flat field, extraction of the orders, wavelength calibration, and cleaning the spectrum from cosmic rays. The normalisation of the spectra to the level of unity was done manually with IRAF⁴. More details about observations carried out with each of the five instruments are provided below.

3.1 FIES

FIES (Fiber-fed Echelle Spectrograph) is a cross-dispersed high-resolution echelle spectrograph mounted on the 2.56-m Nordic Optical Telescope (NOT) at the Observatorio Roque de los Muchachos (ORM) on La Palma, Spain. We used the medium-resolution mode ($R = 46,000$) to observe the bright stars ($10 > V > 7$ mag), and the low-resolution mode ($R = 25,000$), for the faint ones ($11.5 > V > 10$ mag). The observations were carried out by EN and JL. The spectra were reduced and calibrated using the dedicated reduction software *FIEStool* (Stempels 2004) that is based on existing standard IRAF reduction procedures.

3.2 FRESCO

FRESCO is a fiber-linked REOSC echelle spectrograph fed by the 91-cm telescope of the Osservatorio Astrofisico di Catania (INAF-OACt), Italy. The observations were carried out by JM-Ž. The data were reduced and calibrated with IRAF.

3.3 HERMES

HERMES is a fiber-fed echelle spectrograph attached to the Flemish 1.2-m telescope Mercator, also at the ORM (Spain). It is optimised for high resolution, stability, and broad wavelength coverage which is achieved primarily by implementing an image slicer, an anti-fringe CCD coating, and a thermal

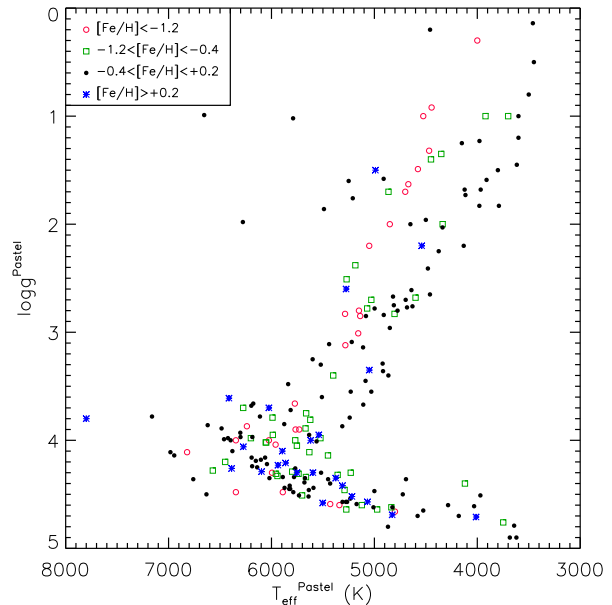


Figure 1. Distribution of the parameters adopted for the reference stars in a $T_{\text{eff}}-\log g$ plane. Stars in different ranges of metallicity are displayed with different colours and symbols.

enclosure (Raskin et al. 2011). The observations were carried out by DD, PL, JG, NG, DV, SB, and CJ. The data reduction and calibration were performed with a dedicated Python-based pipeline (Raskin et al. 2011).

3.4 ESPaDOnS and NARVAL

The ESPaDOnS and the NARVAL spectrographs are very similar to each other. ESPaDOnS is mounted at the 3.6-m Canada-France-Hawaii Telescope (CFHT) at Mauna Kea Observatories (MKO, USA) while NARVAL is mounted at the 2-m T el escope Bernard Lyot (TBL) at the Observatoire Pic du Midi (OPM, France). Both instruments observed the *Kepler* targets in service mode. Data used in the present paper are available in the public archive of the Canada-France-Hawaii Telescope (CFHT) Science Data Archive and the CNRS/INSU CDAB/Bass2000 TBLegacy database. They were reduced and calibrated as part of the service programme by means of the data reduction software Libre-ESPRIT written and provided by J.-F. Donati from IRAP, Observatoire Midi-Pyr en ees (Donati et al. 1997).

4 METHODS OF ANALYSIS

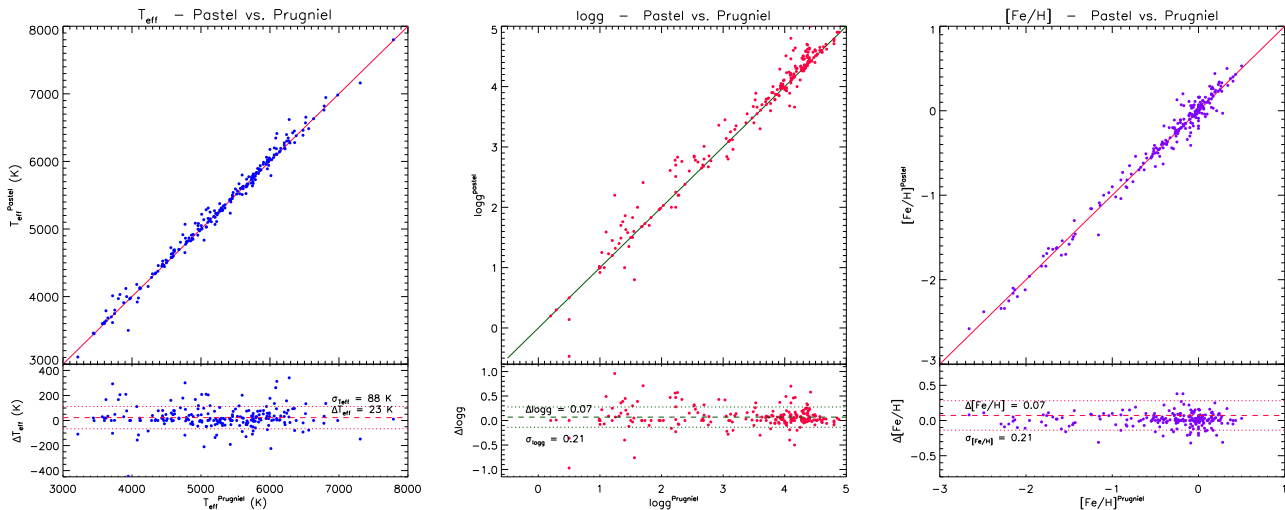
We use two different methods of the spectroscopic analysis, ROTFIT and ARES+MOOG, to derive the atmospheric parameters for our programme stars. As described below, each of these methods makes use of a different approach and has different limitations.

³ <http://planetquest.jpl.nasa.gov/kepler/table>

⁴ IRAF is distributed by the National Optical Astronomy Observatory, which is operated by the Association of Universities for Research in Astronomy, Inc.

Table 1. A summary of instruments and observations.

Instrument	Telescope	Observatory	n	Year of observations	Spectral range [Å]	R	t_{exp} [s]	S/N
FIES	NOT	ORM	4	2010-2011	3700-7300	46,000	420-2050	100 at 4900 Å
FIES	NOT	ORM	6	2010-2011	3700-7300	25,000	1500-2600	100 at 4900 Å
FRESCO	91-cm	INAF-OACt	18	2009-2010	4300-6800	21,000	2700-4200	80 at 6500 Å
HERMES	Mercator	ORM	20	2010-2011	3800-9000	85,000	500-2600	90 at 6500 Å
NARVAL	TBL	OPM	50	2010	3700-10500	75,000	< 900	100 at 5200 Å
ESPaDOnS	CFHT	MKO	91	2010	3700-10500	80,000	< 900	100 at 5200 Å

**Figure 2.** Comparison between the adopted atmospheric parameters (from the PASTEL catalogue, Soubiran et al. 2010) and those from the ELODIE library v3.1 (Prugniel et al. 2007).

4.1 ROTFIT

The code ROTFIT, developed by Frasca et al. (2003, 2006) in IDL⁵ software environment, was originally designed to perform an automatic MK spectral classification and a $v \sin i$ measure by comparing the target spectrum with a grid of slowly-rotating reference spectra. The latter are resampled, aligned to the target spectrum by cross-correlation, and rotationally broadened by convolution with a rotational profile of increasing $v \sin i$ until the minimum of χ^2 is reached. The χ^2 is defined by the following equation:

$$\chi^2 = \frac{1}{N} \sum_j \frac{(y_j^{\text{obs}} - y_j^{\text{templ}})^2}{\sigma_j^2} \quad (1)$$

where y_j^{obs} is the value of the continuum-normalised flux of the observed spectrum at the j^{th} point, y_j^{templ} is the corresponding value for the rotationally-broadened template, σ_j is the error of y_j^{obs} , and N the number of data points.

The code was subsequently used for evaluating, in addition to $v \sin i$, the atmospheric parameters T_{eff} , $\log g$, and $[\text{Fe}/\text{H}]$ by adopting a list of reference stars with well known parameters (see, e.g., Molenda-Żakowicz et al. 2007;

Guillout et al. 2009). A good agreement between the values of T_{eff} , $\log g$, and $[\text{Fe}/\text{H}]$ derived with ROTFIT and those obtained with other techniques are shown, e.g., by Metcalfe et al. (2010); Fröhlich et al. (2012). Unlike codes based on the measurements of equivalent widths and curves of growth, ROTFIT can also be applied to the spectra of FGK stars with $v \sin i$ exceeding 20 km s^{-1} or spectra with a moderate resolution, for which the blending of individual lines prevents the use of the previous methods. Our tests done on a selected sample of spectra of slowly rotating stars artificially broadened by convolution with a rotation profile showed that the derived atmospheric parameters are not significantly affected up to $v \sin i \approx 50 \text{ km s}^{-1}$. For higher values of $v \sin i$, the uncertainties of the atmospheric parameters increase and eventually become as high as 1.5–2 times the original values for $v \sin i = 100 \text{ km s}^{-1}$. As an example of the output produced by ROTFIT for a fast-rotating star (KIC 8677933, G0IV, $v \sin i = 49.6 \text{ km s}^{-1}$), the plot of the observed spectrum and the best-matching template in three spectral regions is shown in Fig. 3. The insets, in which χ^2 for the best template is plotted as a function of $v \sin i$, show that even for such a fast-rotating star the minimum of χ^2 is well defined and that the observed and the template spectra match well.

Our library of reference stars consists of 221 high-resolution ($R = 42,000$), high- S/N spectra of slowly rotating stars acquired with the fiber-fed echelle spectro-

⁵ IDL (Interactive Data Language) is a registered trademark of ITT Visual Information Solutions.

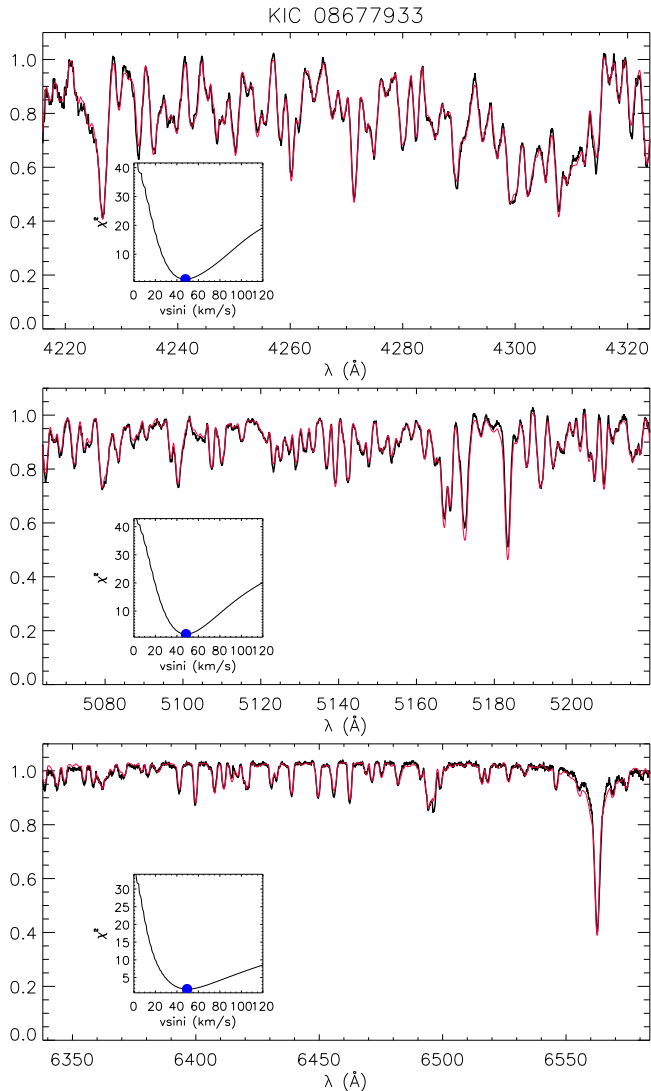


Figure 3. A part of the output of the ROTFIT code for KIC 8677933, a G0IV fast rotating star ($v \sin i = 49.6 \text{ km s}^{-1}$) in three different spectral segments. In each panel, the best template spectrum (thin red line), rotationally broadened and Doppler-shifted, is superimposed onto the observed spectrum of KIC 8677933 (thick black line). The insets show the χ^2 for the best template as a function of $v \sin i$.

graph ELODIE at the Haute-Provence Observatory which are available in the ELODIE archive (Prugniel & Soubiran 2001). The atmospheric parameters of these stars were retrieved from the PASTEL catalogue (Soubiran et al. 2010) and are listed in Table 2. Since for most stars in the PASTEL catalogue there are several determinations of T_{eff} , $\log g$, and $[\text{Fe}/\text{H}]$ obtained by different authors and with different methods, we selected those which are recent, based either on spectral synthesis or on the analysis of the equivalent widths, and which are not significantly different from the bulk of the other determinations. The $T_{\text{eff}}\text{-}\log g$ diagram (Fig. 1) shows that the reference stars are rather well distributed in all the regions relevant for FGK stars with a density that is not certainly uniform, but not very far from it. A comparison between the values of T_{eff} , $\log g$, and $[\text{Fe}/\text{H}]$ adopted by us and those homogeneously re-determined in

the ELODIE library v3.1 by Prugniel et al. (2007) for 220 stars (we note that the latter authors do not provide atmospheric parameters for star GJ 166 C) displays very small offsets and dispersions of 88 K, 0.21 dex, and 0.21 dex for T_{eff} , $\log g$, and $[\text{Fe}/\text{H}]$, respectively (see Fig. 2). That ensures that the adopted parameters are well consistent with those of Prugniel et al. (2007). Table 2 gives also the MK types of our reference stars. Those were adopted either from the SIMBAD database or from the General Catalogue of Stellar Spectral Classifications by Skiff (2013). For most stars that classification agrees with the MK types given for our reference stars in the ELODIE database.

We have analysed independently spectral segments of 100 \AA each or the individual echelle orders, depending on the format of the spectra. We have excluded from the fit the spectral regions heavily affected by telluric lines, like the O_2 band from 6275 to 6330 Å. Per each segment, we took the average parameters of the best ten reference stars ($\sim 5\%$ of the total sample), with a weight proportional to χ^{-2} . Although ROTFIT uses a fixed number of nearest neighbours (10), the weight provided by the χ^2 limits the contamination of the final parameters and allows a meaningful estimate of the uncertainties.

We adopted as the best estimates of T_{eff} , $\log g$, and $[\text{Fe}/\text{H}]$ the weighted averages of the results of each spectral segment using $\sigma_i^{-2} \chi_i^{-2} f_i$ as the weight. Here, σ_i is the standard error of the parameters for the best 10 templates of the i^{th} spectral segment. As such it is adopted as a relative measure of the internal consistency for the i^{th} spectral segment/order, χ_i^{-2} is the minimum chi-square of the i^{th} segment and takes into account differences between orders due to the S/N and the goodness of the fit. The factor f_i , which is an integral over all the i^{th} spectral segment of $(F_\lambda/F_C - 1)$, is proportional to the total line absorption and was included in the weight to correct for the different amount of information contained in different spectral segments. We evaluated the uncertainties of T_{eff} , $\log g$, $[\text{Fe}/\text{H}]$, and $v \sin i$ as the standard errors on the weighted means to which we have summed in quadrature the average dispersion of differences between the stellar parameters of our reference stars given in the PASTEL catalogue and in Prugniel et al. (2007), i.e., $\sigma_{T_{\text{eff}}} = 88 \text{ K}$, $\sigma_{\log g} = 0.21 \text{ dex}$, and $\sigma_{[\text{Fe}/\text{H}]} = 0.21 \text{ dex}$ (see Fig. 2). The MK classification of the target star is performed by adopting the spectral type and the luminosity class of the reference star which more frequently matched with the target spectrum in the different spectral segments.

4.2 ARES+MOOG

This method of analysis allows the derivation of T_{eff} , $\log g$, the microturbulence ξ_t , and $[\text{Fe}/\text{H}]$ following a procedure described and used in (Santos et al. 2004; Sousa et al. 2006, 2008, 2011a,b). Because this method relies on two core codes, namely ARES (Automatic Routine for line Equivalent widths in stellar Spectra) developed by Sousa et al. (2007) and MOOG developed by Sneden (1973), we refer to it as to ARES+MOOG. The method is based on measuring equivalent widths (EW s) of Fe I and Fe II weak absorption lines and then imposing excitation and ionisation equilibrium, assuming LTE approximation. The 2002 version of the code MOOG code is used together with the grid of Atlas 9 plane-parallel model atmospheres (Kurucz 1993). In this

Table 2. The first three rows and the last row of Table 2 which provides the MK type, effective temperature, surface gravity, and metallicity of 221 reference stars used by the ROTFIT code. The atmospheric parameters are adopted mostly from the PASTEL catalogue (Soubiran et al. 2010). The last column provides the references to the sources of the adopted values. The full table is available only in an electronic form.

No	Star Name	Spectral Type	T_{eff}	$\log g$	[Fe/H]	Reference to the Literature
1	BD+023375	F9IVsub	5960	4.04	-2.34	Stephens & Boesgaard (2002), AJ, 123, 1647
2	BD+044551	F7Vw	5730	3.90	-1.70	Tomkin et al. (1992), AJ, 104, 1568
3	BD+174708	sdF8	6025	4.00	-1.63	Fulbright (2000), AJ, 120, 1841
.....
221	HD345957	G0Vwe	5766	3.90	-1.46	Gratton et al. (2003), A&A, 404, 187

procedure, [Fe/H] is a proxy of the metallicity. The equivalent widths are measured automatically with the ARES code which successfully reproduces the manual, interactive determination of *EW*s.

One of the unique characteristics of ARES+MOOG is the list of iron lines. Although a preliminary large list of nearly 500 lines was compiled from the Vienna Atomic Line Database (Kupka et al. 1999), the final list includes around 300 most reliable lines that were carefully tested when automatically measured with ARES (Sousa et al. 2008). Another important aspect of the list is the adopted atomic parameters for each line: The oscillator strengths ($\log gf$) of the lines were recomputed through an inverse analysis of the solar spectrum, allowing in this way to perform a differential analysis relatively to the Sun.

The errors of the parameters derived with ARES+MOOG were obtained by quadratically adding 60 K, 0.1 and 0.04 dex to the method’s intrinsic errors in T_{eff} , $\log g$, and [Fe/H], respectively. Those values were obtained by measuring the typical standard deviation of the parameters discussed by Sousa et al. (2008). A more complete discussion of errors representative for this spectroscopic method can be found in Sousa et al. (2011a).

Since we adopt a differential analysis (using the Sun as the reference), this method is expected to work very well for solar-type stars and to be less accurate for the cooler and the hotter stars, and those which are significantly different from the Sun. For this reason, we don’t provide results for stars cooler than about 4,500 K. Moreover, since ARES+MOOG requires precise measurements of the *EW*s, we do not provide results for stars with $v \sin i > 10 \text{ km s}^{-1}$ because higher rotation causes line blending, preventing precise determination of *EW*. Finally, as ARES+MOOG works best with high-resolution spectra, we do not apply this method to stars observed with $R \leq 25,000$.

5 ATMOSPHERIC PARAMETERS

The values of T_{eff} [K], $\log g$ [cm s^{-2}], [Fe/H] [dex], and $v \sin i$ [km s^{-1}] with their standard deviations, and the MK type derived with ROTFIT are listed in columns 2-10 of Table 3. The values of T_{eff} [K], $\log g$ [cm s^{-2}], [Fe/H] [dex], and ξ_t [km s^{-1}] with their standard deviations derived with ARES+MOOG are listed in columns 11-18. KIC numbers are provided in the first column and the designations of the instrument, in the last but one. The last column contains information about the type of variability of the stars. We

use boldface font for KIC numbers of the stars for which atmospheric parameters are derived for the first time. The boldface font instrument designations indicate that the respective spectrum has not been used in any previous analyses in the literature.

For KIC 9693187 and 11179629, we detected lines of both components in the spectrum. KIC 9025370 was discovered to be a double-lined spectroscopic binary by Thygesen et al. (in preparation). We do not compute the atmospheric parameters for these three stars and we indicate in Table 3 that they are SB2 systems.

For KIC 6370489, 10709834, and 10923629 we do not provide the atmospheric parameters obtained with ARES+MOOG. In the spectrum of the first star we find too few useful spectral lines for ARES+MOOG to converge. In case of KIC 10709834 and 10923629, ARES+MOOG yields very high values of $\log g$ which are not confirmed with ROTFIT. Therefore, we suspect that the results produced by ARES+MOOG for those two stars may be spurious.

Below, we discuss the values of T_{eff} , $\log g$, and [Fe/H] determined with ARES+MOOG and with ROTFIT. We compare these results with each other and with those obtained with the VWA (Versatile Wavelength Analysis) code by Bruntt et al. (2012) and Thygesen et al. (2012) for one hundred stars from our sample. For 145 stars, we compare our temperature determinations with the ones derived with the infrared flux method (IRFM) by Pinsonneault et al. (2012).

5.1 Effective temperature

As shown in Fig. 4, the differences between the values of T_{eff} derived with ARES+MOOG, ROTFIT, VWA and IRFM show various offsets and large standard deviation. The standard deviation is lowest but still significant when the comparisons involve T_{eff} computed with VWA (Fig. 4 *b*, *d*, and *f*). This must be related to the fact that VWA was applied to high-*S/N*, high-resolution spectra from ESPaDOnS and NARVAL: When data of high quality are used, all methods yield T_{eff} which are more precise and accurate

For stars with $T_{\text{eff}} > 6,000 \text{ K}$, the effective temperatures derived with ARES+MOOG are systematically hotter than those obtained with ROTFIT and VWA (Fig. 4 *a* and *b*.) Between 5,000 K and 6,000 K these three methods agree well but for stars cooler than 5,000 K, ARES+MOOG yields slightly higher values of T_{eff} which is why for the coolest stars the agreement between ARES+MOOG and ROTFIT or VWA is worse again. The reason for this may be related to the se-

lection of spectral lines. The original list of lines is optimised for solar-type stars while for cool stars many of those lines are affected by blending. This effect contributes strongly to the observed offset in temperature. A refinement of the selection of lines to produce consistent results for stars cooler than 5,000 K will be presented by Tsantaki et al. (2013).

Fig. 4 *a* and *b* show that when ROTFIT and VWA are compared to ARES+MOOG, the differences show a similar pattern. This suggest that T_{eff} obtained with ROTFIT and VWA should be close to each other. Indeed, the mean difference between T_{eff} derived by means of those two methods is relatively small, only 70 K. Nevertheless, the standard deviation of the differences, 123 K, is still high (Fig. 4 *d*.)

When compared with the IRFM-based T_{eff} measured by Pinsonneault et al. (2012), the values of T_{eff} derived with ARES+MOOG show a negligible offset of 7 K but a high standard deviation of 152 K (Fig. 4 *c*). The two other methods, ROTFIT and VWA, show a much higher mean difference, 182 and 149 K, and similar standard deviation of 179 and 104 K, respectively (Fig. 4 *e* and *f*). Therefore, it is difficult to say which of those methods, if any, agrees with IRFM best.

Since ARES+MOOG temperature scale is known to be in a very good agreement with IRFM (see Sousa et al. 2008), we would expect the results shown in Fig. 4 *c* to agree much better than is the case. One of the plausible explanations of the observed scatter is the fact that the IRFM-based T_{eff} provided by Pinsonneault et al. (2012) were derived only from one colour index, $(J - K_S)$. This index produces the values of T_{eff} which show the highest scatter when compared with the IRFM T_{eff} derived from other colour indices (see Figs. 9-11 in Pinsonneault et al. 2012). Indeed, when the mean values of the IRFM T_{eff} of stars in the Hyades and Praesepe open clusters (computed from $(B - V)$, $(V - I_C)$, and $(V - K_S)$ indices) are compared with the $(J - K_S)$ -based T_{eff} values, and their differences are plotted as a function of the YREC T_{eff} computed by Pinsonneault et al. (2012) by using the isochrones by An et al. (2007), the differences are positive by around 100 K for stars which are cooler than 5900 K and negative by around 50 K for stars which are hotter than 6200 K (see the Fig. 13 in Pinsonneault et al. 2012). The $(J - K_S)$ -based T_{eff} of the *Kepler* stars shown in the same figure show a similar trend as the $(J - K_S)$ -based T_{eff} of stars in Hyades and Praesepe; only for stars hotter than 6200 K their values are closer to the YREC T_{eff} scale (but still lower by around 100 K.)

These results allow us to conclude that the high standard deviation of the differences shown in Fig. 4 *c* is likely due to the calibration issues in the $(J - K_S)$ colour index (c.f. Sect. 3.3 in Pinsonneault et al. 2012), not to any possible weakness of ARES+MOOG. The general consistency of the effective temperatures derived from spectroscopy and the IRFM method is supported also by Bruntt et al. (2012) who show that T_{eff} computed with VWA are in a good agreement with the IRFM T_{eff} values derived from the $V_T - K_S$ index and the calibration of Casagrande et al. (2012) as the mean difference between those two scales of temperature is only 4 ± 85 K (see Bruntt et al. 2012, figure 2) whereas the standard deviation of the differences between VWA-based T_{eff} and those obtained from the $(J - K_S)$ index shown in Fig. 4 *f* is comparable to the value obtained for Fig. 4 *c*.

One should also keep in mind that IRFM T_{eff} de-

rived by Pinsonneault et al. (2012) may be slightly affected by interstellar reddening of the stars: Because there are no individual measurements of $E(B - V)$ for each target, Pinsonneault et al. (2012) correct the observed magnitudes for interstellar extinction using the map-based estimates of extinction from KIC. Unfortunately, those values of $E(B - V)$ are not accurate as has been shown by Molenda-Żakowicz et al. (2009) for 29 nearby ($16 < r < 240$ pc), bright ($9.0 < V < 11.2$) *Kepler* targets which were observed photometrically by those authors. Molenda-Żakowicz et al. (2009) did not find any evidence that those stars were reddened while $E(B - V)$ provided in KIC were sometimes as high as 0.06 mag. The influence of inaccurate $E(B - V)$ used by Pinsonneault et al. (2012) on the IRFM T_{eff} may be small but should be considered as one of possible sources of the scatter in Fig. 4 *c*, *e*, and *f*.

5.2 Metallicity

As shown in Fig. 5 *a*, *b*, and *c*, the values of $[\text{Fe}/\text{H}]$ derived with ARES+MOOG, ROTFIT and VWA agree with each other to within the error bars for almost all targets. The mean differences between these determinations do not exceed 0.07 dex. However, their standard deviations are quite large and comparable to the typical uncertainty of $[\text{Fe}/\text{H}]$ derived with ROTFIT or to twice the typical uncertainty of $[\text{Fe}/\text{H}]$ derived with ARES+MOOG.

For the stars hotter than 6,000 K, the values of $[\text{Fe}/\text{H}]$ derived with ARES+MOOG are slightly higher than those obtained with ROTFIT or VWA (Fig. 5 *a* and *b*). However, this trend does not affect the overall consistency of the results. The values of $[\text{Fe}/\text{H}]$ obtained with ROTFIT and VWA agree best (Fig. 5 *c*) showing a mean difference of 0.03 dex and no trends at high temperatures. The high standard deviation is not reduced, however, and it is as high as that in Fig. 5 *a* where the mean difference is the highest and the trend at the high temperatures is most obvious.

5.3 Surface gravity

The surface gravity is the parameter which is least constrained when derived with ARES+MOOG. The reason for this is related to the number of iron lines used in the method. Although we use nearly 300 Fe I lines, which constrains very well the temperature, microturbulence, and the metal abundance, $\log g$, which comes from the ionisation balance, requires an analysis of Fe II lines. Unfortunately, the number of Fe II lines in our line list is limited to less than 20. Due to that small number, the results of the analysis are more sensitive to errors and more uncertain.

The differences between the $\log g$ values computed with ARES+MOOG, ROTFIT, and VWA illustrated in Fig. 6 *a* and *b*, are around 0.2 dex, and show discrepancies increasing for hot stars. The trends visible in Fig. 6 *a* and *b*, mimic those in Fig. 4 *a* and *b* which may be a result of strong correlations between T_{eff} and $\log g$. The values of $\log g$ obtained with ROTFIT and with VWA agree with each other better (Fig. 6 *c*.) The mean difference between them is the lowest, 0.12 dex, and there are no trends for hot stars. However, the standard deviation of these differences is still high.

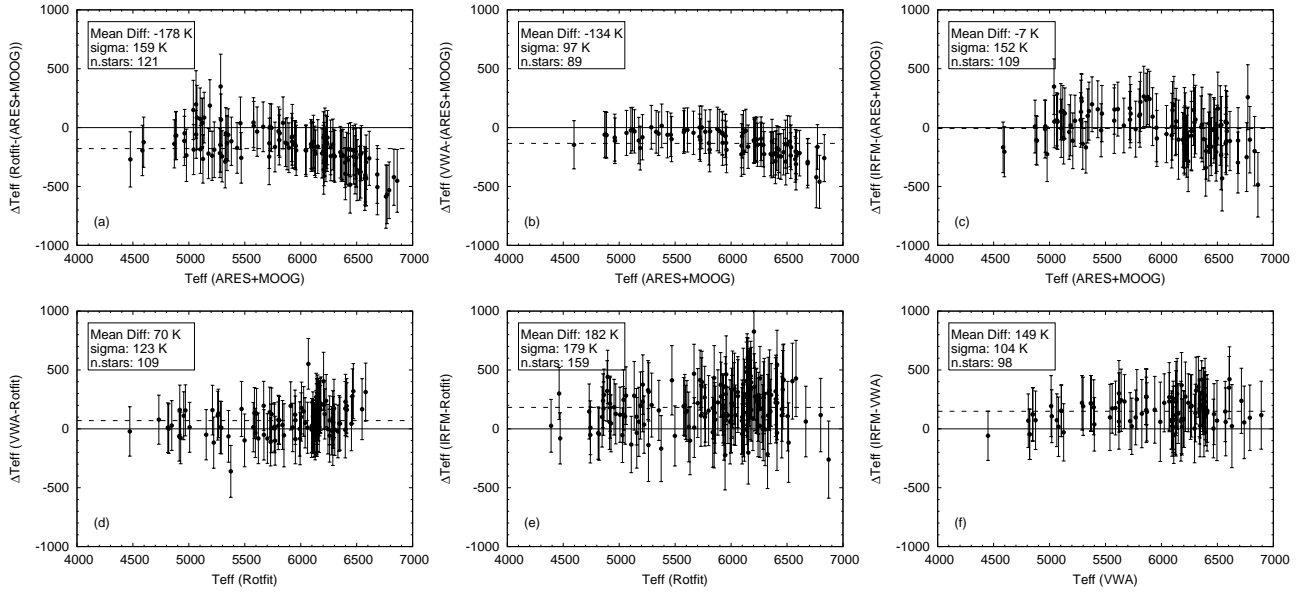


Figure 4. Mutual comparison of T_{eff} values measured with four different methods: ROTFIT and ARES+MOOG (this paper), VWA (Bruntt et al. 2012; Thygesen et al. 2012) and IRFM (Pinsonneault et al. 2012). In the insets, we give the mean difference between the compared sets of data, the standard deviation of the mean, and the number of stars in common.

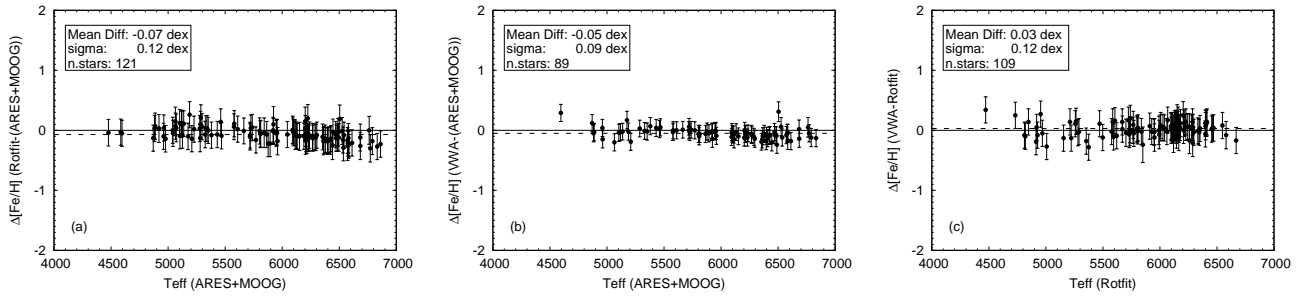


Figure 5. Mutual comparison of $[\text{Fe}/\text{H}]$ values measured with three different methods: ROTFIT and ARES+MOOG (this paper), and VWA (Bruntt et al. 2012; Thygesen et al. 2012). In the insets, we give the mean difference between the compared sets of data, the standard deviation of the mean, and the number of stars in common.

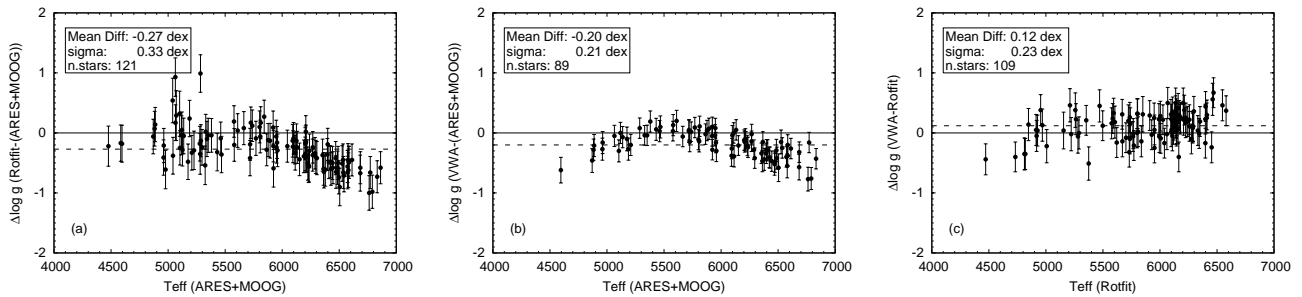


Figure 6. The same as in Fig. 5 but for the $\log g$ values.

6 DISCUSSION

Our analysis shows that deriving precise and accurate atmospheric parameters is not a trivial task and that limiting such determinations to one method can result in a false impression that the accuracy of the atmospheric parameters is as high as is their precision. We showed that while within one method the precision of the computations can be high, when results are compared to those obtained by means of other methods or from different data, various trends and offsets appear, proving that we are not yet able to provide accurate values of T_{eff} , $\log g$, and $[\text{Fe}/\text{H}]$ for solar-type stars.

KIC 5184732 is a good example of those difficulties. In Table 3, we give the atmospheric parameters of that star derived independently from the spectra acquired with FRESCO, ESPaDOnS, and NARVAL. The atmospheric parameters computed with ARES+MOOG from the ESPaDOnS and NARVAL data agree with each other very well. A good consistency in the atmospheric parameters for all the spectra computed with ROTFIT is also found. However, the differences between those two sets of determinations amount to around 150 K in T_{eff} , 0.12 dex in $\log g$, and 0.20 dex in $[\text{Fe}/\text{H}]$. For ROTFIT, there are also less pronounced but still not negligible differences between T_{eff} , $\log g$ and $[\text{Fe}/\text{H}]$ derived from the observations acquired with FRESCO and those obtained with ESPaDOnS and NARVAL.

The trends and discrepancies in the atmospheric parameters observed for stars hotter than 6,000 K represent yet another significant but not a new problem. The problem has been thoroughly discussed, but not solved, by Torres et al. (2012). Those authors compare atmospheric parameters obtained with SPC and SME, two codes in which the method of spectral synthesis is used, with the values of T_{eff} , $\log g$, and $[\text{Fe}/\text{H}]$ computed with MOOG, which uses the curve-of-growth approach. The differences noticed by Torres et al. (2012) are similar to those reported in the present paper. A similar trend can be noticed also in Fig. 3 b, in Sousa et al. (2008), where T_{eff} computed with ARES+MOOG are compared with those obtained with SME. The origin of those discrepancies is not clear but they seem to reflect systematic differences between atmospheric parameters obtained from the spectral synthesis and the analysis of equivalent widths. However, confirming that suspicion would require detailed examination of the input physics used in all the discussed methods which is beyond the scope of this paper.

The comparative analysis which we carried out showed that the currently available accuracy of atmospheric parameters of solar-type stars is ± 150 K in T_{eff} , ± 0.15 dex in $[\text{Fe}/\text{H}]$ and ± 0.3 dex in $\log g$. This applies particularly to faint stars and those hotter than 6,000 K. Since $\log g$ is the parameter most difficult to constrain in spectroscopic analysis, for stars showing solar-like pulsations and those with planetary transits, the seismic $\log g$ or the values of $\log g$ derived from the transit light curves may be used as an alternative value for asteroseismic modelling. Indeed, the $\log g$ values derived from transit light curves (Seager & Mallen-Ornelas 2003) are currently preferred in the investigation of the transiting planets (c.f. Torres et al. 2012) whereas in asteroseismic modelling of stars showing solar-like oscillations, the seismic values of $\log g$ are preferred to the spectroscopic ones (c.f. Morel & Miglio 2012). Another potentially important application of the asteroseis-

mically determined surface gravities may be a validation test for the values of $\log g$ derived from the spectroscopic analyses (see Creevey et al. 2013).

7 SUMMARY

In this paper, we provided two sets of determinations of atmospheric parameters for 169 F, G, K, and M-type stars, dwarfs and giants, with T_{eff} ranging from 3,200 to 6,700 K. The first set was computed with ARES+MOOG, a method based on the analysis of the equivalent widths of spectral lines. The other was derived with ROTFIT, which makes use of the full spectrum by comparison to a grid of reference stars with well-known atmospheric parameters. The latter code was used also to derive the projected rotational velocities of the stars. For 67 stars, the atmospheric parameters (T_{eff} , $\log g$, and $[\text{Fe}/\text{H}]$) are provided for the first time. KIC 9693187 and KIC 11179629 are newly discovered double-lined spectroscopic binary systems.

The typical internal precision of the atmospheric parameters obtained with ARES+MOOG is rather high: ± 80 K, ± 0.12 dex, and ± 0.06 dex in T_{eff} , $\log g$, and $[\text{Fe}/\text{H}]$, respectively. ROTFIT displays a lower internal precision with typical errors of 110 K in T_{eff} , and 0.21 dex in $\log g$ and $[\text{Fe}/\text{H}]$, however, the values of the atmospheric parameters are in good agreement with those derived by Bruntt et al. (2012) and Thygesen et al. (2012). Therefore, we conclude that both ROTFIT and ARES+MOOG produce determinations which can be safely used for asteroseismic modelling of stars or for studying stellar structure and evolution.

Having shown that for solar-type stars the present accuracy of the spectroscopic determinations of atmospheric parameters is ± 150 K in T_{eff} , ± 0.15 dex in $[\text{Fe}/\text{H}]$, and ± 0.3 dex in $\log g$, we emphasise the importance of collecting high-quality spectra with sufficiently large telescopes equipped with efficient spectrographs. We stress also the need of examining reasons why for hot stars the spectral synthesis method and the curve-of-growth analysis yield atmospheric parameters which are systematically different.

ACKNOWLEDGEMENTS

We thank Thierry Louge for help in retrieving the data from the CNRS/INSU CDAB/Bass2000 TBLegacy database operated by the University of Toulouse/OMP, Tarbes, France. We thank the Spanish Night time CAT for awarding the observing time to programs 61-Mercator3/11B, 119-NOT12/11A, and 61-NOT7/10A. J.M.-Ž., E.N., and D.D. acknowledge the Polish MNiSW grant NN203 405139. D.D. acknowledges the Polish National Science Centre grant No. 2011/01/N/ST9/00400. A.F. acknowledges the Italian *Ministero dell'Istruzione, Università e Ricerca* (MIUR). S.G.S., A.M., and M.T. acknowledge the support of the European Research Council/European Community under the FP7 through Starting Grant agreement number 239953. S.G.S. and J.M.-Ž. acknowledge the support from Fundação para a Ciência e a Tecnologia (FCT) through the grant SFRH/BPD/47611/2008, the projects PTDC/CTE-AST/098528/2008, PTDC/CTE-AST/098754/2008, and the 'Cooperação Científica e Tec-

nologica FCT/Polonia 2011/2012 (Proc. 441.00 Polonia)', funded by FCT/MCTES, Portugal and POPH/FSE (EC). SB acknowledges funding from the European Research Council under the European Community's Seventh Framework Programme (FP7/2007–2013)/ERC grant agreement n°227224 (PROSPERITY). KU acknowledges financial support by the Spanish National Plan of R&D for 2010, project AYA2010-17803. M.B. is F.R.S.-FNRS Postdoctoral Researcher, Belgium.

We thank the anonymous Referee for the comments which helped us improve this paper.

REFERENCES

- An D., Terndrup D. M., Pinsonneault M. H., Paulson D. B., Hanson R. B., Stauffer J. R. 2007, *ApJ*, 655, 233
- Appourchaux T., et al. 2012, *A&A*, 543, 54
- Borucki W. J., et al. 2003, in *Society of Photo-Optical Instrumentation Engineers (SPIE) Conference Series*, Vol. 4854, *Society of Photo-Optical Instrumentation Engineers (SPIE) Conference Series*, J. C. Blades, O. H. W. Siegmund, eds., pp. 129140
- Brown T. M., Latham D. W., Everett M. E., Esquerdo G. A. 2011, *AJ*, 142, 112 (<http://cdsarc.u-strasbg.fr/viz-bin/Cat?V/133>)
- Bruntt H., et al. 2012, *MNRAS* 423, 122
- Casagrande L., Ramirez I., Meléndez J., Bessell M., Asplund M. 2010, *A&A* 512, 54
- Chaplin W. J., et al. 2011, *Science*, 332, 213
- Creevey O. L., et al. 2012, *A&A* 537, A111
- Creevey O. L., et al. 2013, *MNRAS*, 431, 2419
- Donati J.-F., Semel M., Carter B. D., Rees D. E., Collier Cameron A. 1997, *MNRAS*, 291, 658
- Frasca A., Alcalà J. M., Covino E., Catalano S., Marilli E., Paladino R. 2003, *A&A*, 405, 149
- Frasca A., Guillout P., Marilli E., Freire Ferrero R., Biazzo K., Klutsch A. 2006, *A&A*, 454, 301
- Frasca A., Fröhlich H.-E., Bonanno A., Catanzaro G., Biazzo K., Molenda-Żakowicz J. 2011, *A&A*, 532, 81
- Fröhlich H.-E., Frasca A., Catanzaro G., Bonanno A., Corsaro E., Molenda-Żakowicz J., Klutsch A., Montes D. 2012, *A&A*, 543, 146
- Gai N., Basu S., Chaplin W. J., Elsworth Y. 2011, *ApJ*, 730, 63
- Guillout P., Schmitt J. H. M. M., Egret D., Voges W., Motch C., Sterzik M. F. 1999, *A&A* 351, 1003
- Guillout P., et al. 2009, *A&A* 504, 829
- Hekker S., et al. 2011, *MNRAS*, 414, 2594
- Høg E., et al. 2000, *A&A*, 355, 27
- Howell S. B., et al. 2012, *ApJ*, 746, 123
- Huber D., et al. 2011, *ApJ*, 743, 143
- Katz D., Soubiran C., Cayrel R., Adda M., Cautain R. 1998, *A&A*, 338, 151
- Koch D. G., et al. 2010, *ApJ*, 713, L79
- Kupka F., Piskunov N., Ryabchikova T. A., Stempels H. C., Weiss W. W. 1999, *A&AS*, 138, 119
- Kurucz R. 1993, *ATLAS9 Stellar Atmosphere Programs and 2 km/s grid*. Kurucz CD-ROM No. 13, Cambridge (Mass.: Smithsonian Astrophysical Observatory)
- Metcalfe T. S., et al. 2010, *ApJ*, 723, 1583
- Molenda-Żakowicz J., et al. 2010, *AN*, 331, 981
- Molenda-Żakowicz J., Frasca A., Latham D. W., Jerzykiewicz M. 2007, *AcA*, 57, 301
- Molenda-Żakowicz J., Kopacki G., Stęślicki M., Narwid A. 2009, *AcA*, 59, 193
- Molenda-Żakowicz J., Latham D. W., Catanzaro G., Frasca A., Quinn S. N. 2011, *MNRAS*, 412, 1210
- Morel T., Miglio A. 2012, *MNRAS*, 419, L34
- Pigulski A., Pojmański G., Pilecki B., Szczygieł D. M. 2009, *AcA*, 59, 33
- Pinsonneault M. H., An D., Molenda-Żakowicz J., Chaplin W. J., Metcalfe T. S., Bruntt H. 2012, *ApJS* 199, 30
- Prugniel Ph., Soubiran C. 2001, *A&A*, 69, 1048
- Prugniel Ph., Soubiran C., Koleva M., Le Borgne D. 2007, *New release of the ELODIE library: Version 3.1*, arXiv:astro-ph/0703658
- Raskin G., et al. 2011, *A&A*, 526, 69
- Santos N. C., Israelian G., Mayor M. 2004, *A&A*, 415, 1153
- Seager S., Mallen-Ornelas G. 2003, *ApJ*, 585, 1038
- Sergey I. 2007, *Perem. Zvezdy Prilozh.*, 7, 2
- Skiff B.A. 2013, *Catalogue of Stellar Spectral Classifications* (Skiff, 2009-2013)
- Smelcer L. 2003, *IBVS*, 5436, 1
- Snedden C. 1973, Ph.D. Thesis, Univ. of Texas <http://www.as.utexas.edu/~chris/moog.html>
- Soubiran C., Katz D., Cayrel R. 1998, *A&AS*, 133, 221
- Soubiran C., Le Campion J.-F., Cayrel de Strobel G., Caillo A. 2010 *A&A* 515, A111
- Sousa S. G., Santos N. C., Israelian G., Mayor M., Monteiro M. J. P. F. G. 2006, *A&A*, 458, 873
- Sousa S. G., Santos N. C., Israelian G., Mayor M., Monteiro M. J. P. F. G. 2007, *A&A*, 469, 783
- Sousa S. G., Santos N. C., Israelian G., Mayor M., Udry S. 2011, *A&A*, 533, A141
- Sousa S. G., Santos N. C., Israelian G., Lovis C., Mayor M., Silva P. B., Udry S. 2011a, *A&A*, 526, A99
- Sousa S. G., Santos N. C., Israelian G., Mayor M., Udry S. 2011b, *A&A*, 533, A141
- Sousa S. G., et al. 2008, *A&A*, 487, 373
- Stello D., et al. 2009, *ApJ* 700, 1589
- Stello D., et al. 2011, *ApJ* 739, 13
- Stempels E. 2004, *FIES Automatic Data Reduction Software* (<http://www.not.iac.es/instruments/fies/fiestool/FIESTool-manual-1.0.pdf>)
- Thygesen A. O., et al. 2012, *A&A*, 543, A160
- Torres G., Fischer D. A., Sozzetti A., Buchhave L. A., Winn J. N., Holman M. J., Carter J. A. 2012, *ApJ*, 757, 161
- Tsantaki M., Sousa S. G., Adibekyan V. Zh., Santos N. C., Mortier A., Israelian G. 2013, *A&A* (in press) (arXiv:1304.6639)
- Uytterhoeven K., et al. 2010a, *AN*, 331, 993
- Uytterhoeven K., et al. 2011, *A&A* 534, 125
- Uytterhoeven K., et al. 2010b, *AN*, 331, P30 (arXiv:1003.6089)
- Verner G. A., et al. 2011, *MNRAS*, 415, 3539

Table 3. The atmospheric parameters, the MK type, and the type of variability of our programme stars. In bold font, we indicate those stars for which the atmospheric parameters are derived for the first time. The symbols and acronyms used for different type of variability are explained in the footnote of this table.

KIC	ROTFIT									ARES+MOOG									Instrument	var
	T_{eff}	σ	$\log g$	σ	[Fe/H]	σ	$v \sin i$	σ	MK	T_{eff}	σ	$\log g$	σ	[Fe/H]	σ	ξ_t	σ			
1430163	6412	123	3.97	0.21	-0.25	0.21	8.1	0.9	F5IV	6833	87	4.70	0.11	0.02	0.06	2.12	0.10	NARVAL	⊙ (1)	
1435467	6169	130	3.95	0.21	-0.04	0.22	9.0	1.0	F8IV	6485	92	4.53	0.13	0.08	0.07	2.02	0.09	NARVAL	⊙ (1)	
2837475	6462	125	3.95	0.23	-0.06	0.21	18.3	1.0	F5IV-V	—	—	—	—	—	—	—	—	ESPaDOnS	⊙ (1)	
3335176	3225	132	1.23	1.25	-0.22	0.21	9.3	2.5	M7II	—	—	—	—	—	—	—	—	FIES	PER (2)	
3424541	6165	108	3.90	0.21	0.13	0.21	24.6	0.8	G0IV	—	—	—	—	—	—	—	—	NARVAL	⊙ (1)	
3427720	5949	98	4.26	0.21	0.00	0.21	2.0	0.7	F9IV-V	6111	68	4.51	0.11	0.04	0.06	1.25	0.04	ESPaDOnS	⊙ (1)	
3430868	4969	101	2.91	0.23	-0.01	0.21	2.6	0.4	G8III	5208	67	3.24	0.12	0.13	0.06	1.46	0.03	ESPaDOnS	⊙ (1)	
3443483	4856	93	3.05	0.21	0.04	0.21	11.1	0.2	K1IV	5043	82	3.43	0.18	0.09	0.06	1.63	0.06	FIES	⊙ (1)	
3456181	6290	111	3.94	0.21	-0.24	0.21	5.0	1.0	F5IV-V	6584	91	4.43	0.11	-0.02	0.07	2.01	0.11	NARVAL	⊙ (1)	
3632418	6148	111	3.94	0.21	-0.19	0.21	6.3	0.5	F6IV	6409	74	4.43	0.12	-0.03	0.06	1.86	0.06	NARVAL	⊙ (1,3)	
3643774	5928	96	4.26	0.22	0.17	0.21	1.4	1.4	G2IV	6125	75	4.39	0.12	0.25	0.06	1.39	0.05	HERMES	⊙ (1)	
3644223	4918	93	3.11	0.24	-0.22	0.21	2.8	0.8	G8III	—	—	—	—	—	—	—	—	FRESCO	⊙ (4)	
3656476	5586	108	4.07	0.21	0.20	0.21	1.4	0.4	G5IV	5719	64	4.26	0.11	0.28	0.05	1.11	0.03	ESPaDOnS	⊙ (1)	
3733735	6548	156	3.99	0.22	-0.12	0.21	13.0	1.4	F5IV-V	—	—	—	—	—	—	—	—	ESPaDOnS	⊙ (1)	
3747220	6668	147	4.18	0.21	0.00	0.21	50.8	12.4	F3V	—	—	—	—	—	—	—	—	ESPaDOnS	⊙ (1)	
4072740	4847	94	3.08	0.23	0.09	0.21	1.6	0.3	K1IV	4960	77	3.49	0.13	0.19	0.06	1.13	0.06	NARVAL	⊙ (1)	
4346201	6154	109	3.98	0.22	-0.25	0.21	2.8	1.0	F8V	6239	91	4.28	0.12	-0.17	0.07	1.64	0.10	HERMES	⊙ (1)	
4586099	6304	109	3.92	0.21	-0.20	0.21	2.3	0.7	F5IV-V	6533	80	4.37	0.11	-0.04	0.06	1.84	0.08	ESPaDOnS	⊙ (1)	
4638884	6286	123	3.91	0.21	-0.17	0.21	4.6	0.8	F5IV-V	6684	98	4.58	0.17	-0.05	0.08	3.39	0.28	NARVAL	⊙ (1)	
4859338	6013	131	4.09	0.23	0.19	0.21	34.3	1.5	G0IV	—	—	—	—	—	—	—	—	HERMES	⊙ (13)	
4914923	5808	92	4.28	0.21	0.13	0.21	2.3	0.8	G1.5V	5948	65	4.34	0.12	0.18	0.05	1.26	0.03	ESPaDOnS	⊙ (1)	
4931363	7045	128	4.07	0.22	-0.05	0.21	65.9	8.0	F0III	—	—	—	—	—	—	—	—	ESPaDOnS	⊙ (1)	
4931390	6410	160	3.97	0.21	-0.25	0.21	3.2	1.2	F5IV-V	6862	80	4.55	0.11	-0.02	0.06	1.93	0.09	ESPaDOnS	⊙ (1)	
5021689	6141	107	3.94	0.21	-0.16	0.22	7.0	0.6	F8IV	6378	80	4.55	0.13	-0.02	0.06	1.90	0.08	ESPaDOnS	⊙ (1)	
5024851	4046	92	1.77	0.21	-0.18	0.21	1.9	0.7	K4III	—	—	—	—	—	—	—	—	ESPaDOnS	⊙ (5)	
5080290	5157	169	3.60	0.35	-0.06	0.22	4.6	0.9	K0III-IV	5072	77	3.31	0.16	-0.10	0.07	0.69	0.07	HERMES	δ Sct (6)	
...	5261	182	4.21	0.26	0.01	0.23	6.1	0.5	K0III-IV	5064	78	3.28	0.13	-0.14	0.06	0.79	0.06	ESPaDOnS	⊙ (1)	
5112786	4207	92	1.99	0.21	-0.17	0.21	2.5	0.9	K3III	4477	114	2.21	0.22	-0.13	0.07	1.83	0.08	ESPaDOnS	⊙ (1)	
5184732	5669	97	4.07	0.21	0.24	0.21	2.8	0.3	G4V	—	—	—	—	—	—	—	—	FRESCO	⊙ (1)	
...	5723	103	4.18	0.23	0.21	0.21	2.2	0.6	G4V	5894	68	4.31	0.12	0.43	0.06	1.18	0.03	ESPaDOnS*	⊙ (1)	
...	5740	115	4.22	0.22	0.18	0.21	2.4	0.5	G1V	5877	68	4.34	0.11	0.40	0.06	1.14	0.03	NARVAL*	⊙ (1)	
5199859	3722	133	1.63	0.35	-0.07	0.21	10.8	1.3	M0III	—	—	—	—	—	—	—	—	FIES	⊙ (1)	
5371516	6138	90	3.98	0.22	0.10	0.21	9.7	1.2	F8IV	6526	107	4.49	0.15	0.11	0.08	2.35	0.14	ESPaDOnS	⊙ (1)	
5450445	6099	99	4.13	0.21	0.05	0.21	5.4	0.6	F8V	6396	75	4.49	0.11	0.23	0.06	1.75	0.06	NARVAL	⊙ (1)	
5512589	5764	95	4.22	0.21	0.06	0.21	1.6	0.4	G3V	5812	66	4.05	0.11	0.12	0.06	1.20	0.03	NARVAL	⊙ (1)	
5557932	5936	100	4.37	0.21	0.00	0.21	13.7	0.3	G1.5V	—	—	—	—	—	—	—	—	ESPaDOnS	RS CVn (7)	
5596656	5375	112	3.99	0.24	-0.18	0.21	3.8	0.4	G5IV	5188	69	3.75	0.13	-0.44	0.06	1.05	0.05	ESPaDOnS	⊙ (1)	
5620305	5190	148	3.49	0.32	-0.01	0.21	4.2	1.1	K0III-IV	5040	70	2.95	0.12	-0.01	0.06	0.51	0.05	HERMES	⊙ (1)	
5701829	4927	104	3.19	0.22	-0.24	0.21	2.3	0.5	K0IV	—	—	—	—	—	—	—	—	FRESCO	⊙ (1)	
...	4914	92	3.18	0.22	-0.13	0.21	2.4	0.7	K0IV	4962	69	3.39	0.13	-0.17	0.06	1.13	0.04	ESPaDOnS	⊙ (1)	
5737655	5163	101	2.88	0.25	-0.44	0.21	3.8	0.6	G4III-IV	5121	63	2.83	0.10	-0.56	0.05	1.68	0.02	ESPaDOnS	⊙ (1)	
5773345	6007	112	4.17	0.21	0.13	0.21	3.4	1.1	G0.5IV	6399	71	4.36	0.11	0.30	0.06	1.92	0.05	ESPaDOnS	⊙ (1)	

Table 3. continuation.

KIC	T_{eff}	σ	$\log g$	σ	[Fe/H]	σ	$v \sin i$	σ	MK	T_{eff}	σ	$\log g$	[Fe/H]	σ	ξ_t	σ	Instrument	var	
					ROTFIT								ARES+MOOG						
5774694	5804	91	4.34	0.21	0.08	0.21	3.6	0.5	G2V	5923	65	4.56	0.10	0.10	0.05	1.17	0.03	ESPaDOnS*	⊙ (1)
...	5801	98	4.34	0.21	0.06	0.21	3.6	0.6	G3V	5950	64	4.58	0.10	0.09	0.05	1.19	0.03	NARVAL*	
5952403	5058	106	2.99	0.26	0.01	0.21	13.6	0.1	G8III	—	—	—	—	—	—	—	—	FIES	
5955122	5952	100	4.13	0.21	-0.05	0.22	4.5	0.6	F9IV-V	6092	69	4.26	0.12	-0.06	0.06	1.66	0.05	ESPaDOnS	⊙ (1)
6116048	5991	124	4.09	0.22	-0.24	0.23	2.9	0.6	F9IV-V	6152	66	4.53	0.10	-0.14	0.05	1.36	0.04	ESPaDOnS	⊙ (1)
6225718	6138	106	3.96	0.21	-0.23	0.22	2.4	0.5	F8V	6366	70	4.61	0.11	-0.07	0.06	1.50	0.05	NARVAL	⊙ (1)
6285677	5849	97	4.32	0.22	0.06	0.22	7.6	1.0	G2V	6205	73	4.48	0.11	0.23	0.06	1.48	0.05	HERMES	
...	5907	94	4.18	0.21	0.02	0.21	7.8	0.9	G0.5IV	—	—	—	—	—	—	—	—	FRESCO	
6370489	6241	116	3.98	0.21	-0.35	0.21	4.4	0.8	F8V	—	—	—	—	—	—	—	—	FIES	⊙ (1)
6442183	5736	96	4.26	0.21	-0.07	0.21	1.7	0.5	G1V	5738	62	4.14	0.10	-0.12	0.05	1.15	0.02	NARVAL	⊙ (1)
6508366	6332	117	3.91	0.21	-0.07	0.21	18.0	1.0	F6IV	—	—	—	—	—	—	—	—	ESPaDOnS	⊙ (1)
6590668	4463	93	2.02	0.22	-0.22	0.21	4.0	1.1	K1III	—	—	—	—	—	—	—	—	FRESCO	
6603624	5471	128	4.02	0.23	0.17	0.21	1.4	0.7	G8IV-V	5718	78	4.44	0.13	0.28	0.06	1.16	0.06	ESPaDOnS	⊙ (1)
6679371	6344	131	3.92	0.21	-0.10	0.21	11.0	1.0	F5IV-V	—	—	—	—	—	—	—	—	NARVAL	⊙ (1)
6766118	4892	93	2.73	0.21	0.05	0.21	2.7	0.6	K0III	—	—	—	—	—	—	—	—	FRESCO	
6933899	5837	97	4.21	0.22	0.04	0.21	2.0	0.6	G0.5IV	5921	65	4.12	0.11	0.04	0.06	1.29	0.03	NARVAL	⊙ (1)
7103006	6180	120	3.92	0.21	-0.07	0.22	8.9	0.6	F8IV	6685	86	4.50	0.11	0.19	0.06	1.98	0.08	NARVAL	⊙ (1)
7206837	6142	112	4.05	0.21	0.05	0.21	6.7	0.5	F8IV	6573	80	4.61	0.11	0.22	0.06	1.93	0.06	NARVAL	⊙ (1)
7282890	6207	97	3.89	0.22	0.02	0.21	21.0	1.0	F6IV	—	—	—	—	—	—	—	—	ESPaDOnS	⊙ (1)
7510397	6120	97	3.94	0.21	-0.26	0.22	2.2	0.8	F6IV	6362	80	4.54	0.12	-0.08	0.06	1.66	0.07	ESPaDOnS	⊙ (1)
7529180	6470	128	4.03	0.21	-0.06	0.21	27.0	1.7	F5IV-V	—	—	—	—	—	—	—	—	NARVAL	⊙ (1)
7662428	6143	97	4.03	0.21	0.10	0.21	9.3	0.8	F8V	6504	141	4.93	0.19	-0.09	0.10	1.58	0.22	ESPaDOnS	⊙ (13)
7668623	6159	105	3.94	0.21	-0.10	0.23	7.6	0.7	F8IV	6580	112	4.56	0.15	0.03	0.08	2.54	0.21	ESPaDOnS	⊙ (1)
7680114	5799	91	4.25	0.21	0.08	0.21	1.4	0.8	G0V	5955	68	4.41	0.11	0.12	0.06	1.30	0.04	NARVAL	⊙ (1)
7730305	6060	104	4.25	0.22	0.09	0.21	12.6	1.1	F8V	6304	81	4.67	0.11	0.17	0.06	1.69	0.07	HERMES	
...	6030	104	4.17	0.21	0.01	0.21	15.0	0.8	F8V	—	—	—	—	—	—	—	—	FRESCO	
7747078	5994	113	4.04	0.23	-0.19	0.23	3.8	0.8	F9IV-V	6114	78	4.37	0.12	-0.11	0.06	1.65	0.07	ESPaDOnS	⊙ (1)
7799349	4954	92	3.33	0.22	0.14	0.21	1.1	0.4	K1IV	5175	84	3.81	0.15	0.24	0.07	1.31	0.07	NARVAL	⊙ (1)
7799575	3941	92	1.69	0.21	-0.17	0.21	2.2	0.7	K5III	—	—	—	—	—	—	—	—	ESPaDOnS	Mira (8)
7800289	6398	133	3.96	0.21	-0.17	0.21	18.6	1.1	F5IV	—	—	—	—	—	—	—	—	NARVAL	⊙ (9)
7871531	5498	117	4.31	0.21	-0.12	0.21	2.2	0.8	G5V	5461	67	4.40	0.12	-0.26	0.06	0.87	0.05	ESPaDOnS	⊙ (1)
7940546	6243	101	3.92	0.21	-0.25	0.21	6.6	0.8	F6IV	6427	82	4.52	0.12	-0.11	0.06	2.09	0.09	ESPaDOnS*	⊙ (1)
...	6226	119	3.94	0.21	-0.24	0.21	7.0	0.7	F6IV	6472	84	4.59	0.12	-0.11	0.06	2.32	0.12	NARVAL*	
7970740	5354	111	4.36	0.21	-0.31	0.21	2.4	0.5	G9V	5287	68	4.49	0.11	-0.52	0.05	0.59	0.08	ESPaDOnS	⊙ (1)
7976303	6119	106	3.97	0.21	-0.38	0.21	3.1	0.5	F8V	6203	76	4.15	0.11	-0.41	0.06	1.62	0.07	ESPaDOnS	⊙ (1)
7985370	5836	103	4.39	0.21	0.02	0.21	16.4	0.3	G1.5V	—	—	—	—	—	—	—	—	HERMES	PER (2)
...	5849	90	4.28	0.21	-0.10	0.21	17.3	0.4	G1.5V	—	—	—	—	—	—	—	—	FRESCO	rot/act (6,11)
8006161	5258	97	4.13	0.25	0.23	0.21	2.0	0.5	G8V	5431	82	4.45	0.13	0.30	0.06	0.95	0.10	ESPaDOnS*	⊙ (1)
...	5211	101	4.05	0.24	0.20	0.21	1.9	0.3	G8V	5468	77	4.41	0.13	0.29	0.06	1.07	0.07	NARVAL*	
8026226	6276	94	3.90	0.21	-0.20	0.21	7.4	0.5	F5IV-V	6469	78	4.32	0.13	-0.13	0.06	2.72	0.18	ESPaDOnS	⊙ (9)
8179536	6160	112	3.98	0.21	-0.16	0.21	8.1	0.6	F6IV	6536	74	4.64	0.11	0.13	0.06	1.61	0.05	NARVAL	⊙ (1)

Table 3. continuation.

KIC	ROTFIT								ARES+MOOG								Instrument	var	
	T_{eff}	σ	$\log g$	σ	[Fe/H]	σ	$v \sin i$	σ	MK	T_{eff}	σ	$\log g$	σ	[Fe/H]	σ	ξ_t			σ
8211551	4812	93	2.83	0.23	-0.12	0.21	1.9	0.5	G9III	4882	68	2.76	0.12	-0.15	0.06	1.54	0.03	ESPaDOnS*	
...	4820	93	2.83	0.22	-0.10	0.21	2.0	0.3	G9III	4887	70	2.69	0.13	-0.17	0.06	1.56	0.03	NARVAL*	
8228742	6061	108	4.02	0.22	-0.12	0.21	3.3	1.1	F9IV-V	6295	76	4.42	0.11	0.00	0.06	1.71	0.06	ESPaDOnS	⊙ (1)
8343931	6506	125	4.09	0.22	-0.03	0.21	43.2	4.0	F5IV-V	—	—	—	—	—	—	—	—	ESPaDOnS	
8346342	6141	119	3.93	0.21	-0.05	0.22	6.9	0.8	F8IV	6573	139	4.59	0.12	0.21	0.10	1.87	0.15	ESPaDOnS	
8352528	3972	89	1.69	0.21	-0.18	0.21	2.2	0.9	K5III	—	—	—	—	—	—	—	—	ESPaDOnS	
8360349	6176	91	3.92	0.21	0.07	0.21	10.6	0.7	F8IV	6762	156	4.92	0.15	0.07	0.10	3.45	0.37	ESPaDOnS	⊙ (1)
8367710	6227	116	3.92	0.21	0.02	0.21	15.0	1.1	F6IV	—	—	—	—	—	—	—	—	ESPaDOnS	⊙ (1)
8379927	5998	108	4.25	0.21	-0.03	0.22	8.8	0.8	F9IV-V	6225	95	4.76	0.13	-0.23	0.07	2.01	0.13	ESPaDOnS*	⊙ (1)
...	6000	112	4.12	0.22	-0.05	0.23	13.0	2.0	F9IV-V	6202	73	4.47	0.12	-0.20	0.06	0.95	0.05	NARVAL*	
8394589	6111	116	3.98	0.21	-0.37	0.21	4.4	0.8	F8V	6231	75	4.54	0.11	-0.24	0.06	1.36	0.07	NARVAL	⊙ (1)
8429280	5029	103	4.35	0.21	-0.04	0.21	34.8	0.6	K2V	—	—	—	—	—	—	—	—	FRESCO	rot/act (12)
...	5108	114	4.56	0.23	0.06	0.21	33.2	1.0	K1V	—	—	—	—	—	—	—	—	HERMES	
8491147	5007	95	2.92	0.24	-0.24	0.21	2.5	0.6	G8III	5065	65	2.75	0.12	-0.31	0.06	1.57	0.02	ESPaDOnS	⊙ (4)
8524425	5671	105	4.17	0.22	0.12	0.21	1.1	0.5	G2.5V	5664	65	4.09	0.11	0.13	0.05	1.16	0.03	NARVAL	⊙ (1)
8542853	5594	99	4.34	0.21	-0.09	0.21	2.1	0.6	G6V	5580	68	4.54	0.12	-0.20	0.06	0.85	0.06	ESPaDOnS	
8547390	4732	90	2.80	0.21	-0.01	0.21	3.0	0.3	K0III	4870	74	2.86	0.15	0.12	0.06	1.60	0.04	ESPaDOnS	⊙ (1)
8561221	5290	115	3.76	0.23	-0.04	0.21	1.9	0.6	G9.5IV	5352	68	3.80	0.11	-0.04	0.06	1.14	0.04	NARVAL	⊙ (1)
8579578	6297	144	3.91	0.21	-0.06	0.21	19.3	1.0	F6IV	—	—	—	—	—	—	—	—	NARVAL	⊙ (1)
8677933	5946	161	3.92	0.29	0.15	0.22	49.6	0.7	G0IV	—	—	—	—	—	—	—	—	ESPaDOnS	⊙ (1)
8694723	6258	117	3.97	0.21	-0.42	0.21	4.6	1.0	G0IV	6445	80	4.55	0.11	-0.39	0.06	1.91	0.11	NARVAL	⊙ (1)
...	6287	116	4.00	0.21	-0.38	0.22	3.8	0.7	G0IV	6489	85	4.50	0.13	-0.35	0.06	1.98	0.13	FIES	
8702606	5621	106	4.08	0.21	0.00	0.21	0.7	0.7	G5IV-V	5578	62	3.89	0.10	-0.06	0.05	1.16	0.02	ESPaDOnS	⊙ (1)
8738809	6039	104	4.19	0.21	0.07	0.21	2.2	0.9	G0.5IV	6207	68	4.17	0.11	0.12	0.06	1.65	0.03	NARVAL	⊙ (1)
8751420	5281	115	3.86	0.24	-0.11	0.21	1.1	0.5	G8IV	5330	62	3.84	0.10	-0.14	0.05	1.07	0.02	NARVAL	⊙ (1)
8760414	5850	166	3.94	0.26	-0.90	0.29	3.4	2.3	G0IV	5924	77	4.53	0.11	-1.00	0.06	1.38	0.11	NARVAL	⊙ (1)
8816903	7063	142	4.12	0.21	-0.05	0.21	57.6	5.0	F0V	—	—	—	—	—	—	—	—	ESPaDOnS	
8831759	3877	107	1.66	0.24	-0.11	0.21	2.4	0.7	M1III	4920	209	3.94	0.34	-0.14	0.10	3.65	0.58	ESPaDOnS	
8866102	6195	134	3.95	0.21	-0.16	0.21	11.0	0.8	F6IV	—	—	—	—	—	—	—	—	ESPaDOnS	⊙? (10)
8938364	5702	101	4.25	0.21	-0.16	0.22	2.0	0.9	G3V	5808	71	4.31	0.12	-0.10	0.06	1.10	0.05	NARVAL	⊙ (1)
9025370	—	—	—	—	—	—	—	—	—	—	—	—	—	—	—	—	—	ESPaDOnS	⊙ SB2 (1,14)
9098294	5766	96	4.27	0.21	-0.22	0.22	2.6	0.6	G3V	5959	80	4.56	0.12	-0.04	0.06	1.13	0.07	NARVAL	⊙ (1)
9116461	6358	108	3.95	0.21	-0.14	0.21	14.1	0.6	F5IV-V	—	—	—	—	—	—	—	—	ESPaDOnS	⊙ (1)
9139151	6004	94	4.26	0.21	0.07	0.21	3.2	0.5	G0.5IV	6213	67	4.64	0.11	0.17	0.06	1.24	0.04	ESPaDOnS	⊙ (1)
9139163	6175	123	3.99	0.22	0.00	0.21	2.0	1.0	F8IV	6577	69	4.44	0.10	0.21	0.06	1.68	0.04	ESPaDOnS*	⊙ (1)
...	6151	128	3.98	0.21	-0.05	0.22	1.9	0.8	F8IV	6584	67	4.47	0.11	0.19	0.05	1.70	0.03	NARVAL*	
9206432	6204	142	3.95	0.21	-0.02	0.22	1.7	1.2	F8IV	6772	73	4.61	0.11	0.28	0.06	1.92	0.05	ESPaDOnS	⊙ (1)
9226926	6580	142	4.12	0.21	-0.15	0.22	30.8	3.0	F5V	—	—	—	—	—	—	—	—	NARVAL	⊙ (1)
9289275	5931	103	4.25	0.22	0.07	0.22	2.7	1.5	G0.5IV	6208	77	4.40	0.12	0.20	0.06	1.51	0.06	HERMES	⊙ (1)
9414417	6242	104	3.92	0.21	-0.19	0.21	6.0	1.1	F6IV	6496	124	4.66	0.13	-0.07	0.09	2.55	0.26	HERMES	⊙ ⚡? (1,10)
9512063	5882	112	4.14	0.22	-0.19	0.24	2.5	1.3	F9IV-V	5842	72	3.87	0.11	-0.15	0.06	1.12	0.04	HERMES	⊙ (1)
9514879	5971	92	4.31	0.21	0.02	0.21	10.1	0.3	G1.5V	6190	79	4.70	0.12	0.12	0.06	1.60	0.07	FIES	
9532030	4472	92	2.35	0.22	-0.11	0.21	3.6	0.5	G9III	4596	85	2.53	0.17	-0.06	0.06	1.74	0.06	ESPaDOnS	

Table 3. continuation.

KIC	T_{eff}	σ	$\log g$	σ	ROTFIT				MK	ARES+MOOG								Instrument	var
					[Fe/H]	σ	$v \sin i$	σ		T_{eff}	σ	$\log g$	σ	[Fe/H]	σ	ξ_t	σ		
9534041	5061	96	3.10	0.23	0.02	0.21	3.2	0.6	G8III	5278	72	3.28	0.12	-0.01	0.06	1.49	0.04	ESPaDOnS	⊙ (5)
9605196	4455	90	1.91	0.23	-0.20	0.21	3.5	0.8	K1III	—	—	—	—	—	—	—	—	FRESCO	
9655101	5039	129	3.02	0.26	0.00	0.21	3.5	0.7	G8III	5227	73	3.31	0.13	-0.02	0.06	1.53	0.04	ESPaDOnS	⊙ (5)
9655167	5036	109	3.03	0.25	-0.01	0.21	4.5	0.5	G8III	5325	80	3.57	0.15	0.06	0.07	1.57	0.06	ESPaDOnS	⊙ (5)
9693187	—	—	—	—	—	—	—	—	—	—	—	—	—	—	—	—	—	ESPaDOnS	⊙ SB2 (1,15)
9700679	5176	158	3.37	0.32	0.04	0.22	3.7	0.9	G8III	5101	73	3.05	0.13	-0.08	0.06	1.01	0.04	HERMES	hybrid (6)
9702369	5956	132	4.04	0.22	-0.11	0.23	5.1	1.4	F9IV-V	6441	78	4.54	0.11	0.14	0.06	1.39	0.05	HERMES	⊙ (1)
9715099	6180	93	4.07	0.21	0.07	0.22	25.1	1.2	F6IV	—	—	—	—	—	—	—	—	FRESCO	⊙ (1)
9716090	5053	106	3.17	0.24	0.02	0.21	3.3	0.6	G8III	5297	74	3.41	0.12	-0.04	0.06	1.75	0.05	ESPaDOnS	⊙ (5)
9716522	4860	92	2.82	0.21	-0.03	0.21	2.7	0.3	G9III	5126	73	3.10	0.12	0.05	0.06	1.67	0.04	ESPaDOnS	⊙ (5)
9812850	6258	97	3.94	0.21	-0.22	0.21	9.8	0.7	F6IV	6790	118	4.92	0.13	-0.04	0.08	2.70	0.27	ESPaDOnS	⊙ (1)
9908400	6068	106	3.95	0.22	0.17	0.21	17.9	0.9	G0IV	—	—	—	—	—	—	—	—	NARVAL	⊙ (1)
9955598	5264	95	4.29	0.22	-0.04	0.21	1.2	0.6	K0V	5380	68	4.33	0.12	0.04	0.06	0.80	0.06	NARVAL	⊙ $\varphi?$ (1,10)
9965715	6326	116	4.00	0.21	-0.30	0.21	8.2	0.7	F2V	6542	87	4.71	0.12	-0.22	0.06	1.84	0.10	ESPaDOnS	
10001154	4391	96	2.17	0.22	-0.23	0.21	2.6	0.2	G9III	4585	82	2.34	0.16	-0.20	0.06	2.06	0.06	ESPaDOnS	
10010623	6464	106	4.11	0.21	-0.01	0.21	31.8	2.1	F3V	—	—	—	—	—	—	—	—	ESPaDOnS	
10016239	6214	103	3.95	0.21	-0.17	0.21	10.7	1.0	F6IV	—	—	—	—	—	—	—	—	NARVAL	⊙ (1)
10018963	6145	112	3.95	0.21	-0.27	0.21	2.1	0.6	F6IV	6354	69	4.32	0.11	-0.16	0.05	1.79	0.05	NARVAL	⊙ (1)
10068307	6144	109	3.94	0.21	-0.22	0.21	3.4	0.8	F6IV	6288	68	4.28	0.10	-0.11	0.06	1.68	0.04	ESPaDOnS	⊙ (1)
10079226	5854	97	4.27	0.21	0.10	0.21	1.6	1.2	G0V	6045	68	4.49	0.11	0.17	0.06	1.17	0.04	HERMES	⊙ (1)
10124866	5736	92	4.29	0.21	-0.31	0.21	3.0	0.6	G4V	5864	68	4.57	0.11	-0.24	0.06	1.03	0.05	ESPaDOnS	⊙ (9)
10131030	4897	89	2.74	0.21	0.02	0.21	3.0	0.9	G8III	—	—	—	—	—	—	—	—	FRESCO	
10162436	6149	115	3.95	0.21	-0.16	0.22	2.8	0.8	F8IV	6423	71	4.43	0.11	0.01	0.06	1.75	0.05	ESPaDOnS	⊙ (1)
10355856	6351	118	3.93	0.21	-0.22	0.21	4.5	0.8	F5IV-V	6612	79	4.38	0.11	-0.01	0.06	1.84	0.05	ESPaDOnS	⊙ (1)
10388249	4743	92	2.87	0.22	0.00	0.21	10.6	0.2	K1IV	4978	98	3.48	0.19	0.14	0.07	1.87	0.09	FIES	⊙ (1)
10454113	6129	151	4.07	0.22	-0.16	0.22	3.7	1.0	F9IV-V	6216	68	4.46	0.10	0.00	0.05	1.30	0.04	ESPaDOnS	⊙ (1)
10462940	6026	101	4.24	0.21	0.05	0.21	1.9	0.7	G0.5IV	6268	68	4.48	0.10	0.18	0.05	1.35	0.03	NARVAL	⊙ (1)
10516096	5928	95	4.24	0.21	-0.04	0.21	2.8	0.6	F9IV-V	6094	70	4.47	0.11	-0.03	0.06	1.39	0.05	ESPaDOnS	⊙ (1)
10526137	3316	274	3.93	0.57	-0.23	0.21	13.4	1.6	M2V	—	—	—	—	—	—	—	—	FIES	APER (2)
10644253	5910	93	4.30	0.21	0.05	0.21	1.6	0.7	G0V	6132	65	4.54	0.11	0.15	0.05	1.21	0.03	ESPaDOnS	⊙ (1)
10709834	6398	124	3.94	0.21	-0.20	0.21	7.0	1.2	F5IV-V	—	—	—	—	—	—	—	—	NARVAL	⊙ (1)
10735274	3836	202	1.72	0.36	-0.06	0.22	2.8	1.5	K5III	—	—	—	—	—	—	—	—	HERMES	
...	4033	99	1.69	0.23	-0.17	0.20	9.3	2.0	K4III	—	—	—	—	—	—	—	—	FRESCO	
10923629	6109	99	4.00	0.21	0.08	0.21	7.3	0.8	F8V	—	—	—	—	—	—	—	—	NARVAL	⊙ (1)
10963065	6097	130	4.00	0.21	-0.27	0.22	2.3	0.6	F8V	6236	64	4.55	0.11	-0.15	0.05	1.47	0.03	NARVAL	⊙ $\varphi?$ (1,10)
11018874	6454	121	4.08	0.21	-0.04	0.21	49.0	2.3	F5V	—	—	—	—	—	—	—	—	ESPaDOnS	
11026764	5771	97	4.22	0.21	0.10	0.21	2.6	0.9	G1V	5802	68	4.12	0.11	0.11	0.06	1.30	0.04	ESPaDOnS	⊙ (1)
11037105	6801	132	4.20	0.22	-0.14	0.23	27.9	2.0	F2V	—	—	—	—	—	—	—	—	ESPaDOnS	
11081729	6400	127	3.97	0.21	-0.19	0.22	21.4	0.7	F5IV	—	—	—	—	—	—	—	—	ESPaDOnS	⊙ (1)
11099165	3930	90	1.69	0.21	-0.18	0.21	2.5	0.7	K5III	—	—	—	—	—	—	—	—	ESPaDOnS	
11137075	5576	99	4.14	0.22	-0.04	0.21	2.3	0.4	G5IV-V	5610	71	4.10	0.12	-0.06	0.06	1.10	0.04	NARVAL	⊙ (1)
11244118	5605	104	4.05	0.23	0.19	0.21	1.7	0.5	G5IV	5770	67	4.14	0.11	0.35	0.06	1.19	0.03	NARVAL	⊙ (1)
11253226	6410	125	3.96	0.21	-0.20	0.21	11.4	1.2	F5IV-V	—	—	—	—	—	—	—	—	ESPaDOnS	⊙ (1)

Table 3. continuation.

KIC	T_{eff}	σ	$\log g$	σ	ROTFIT					ARES+MOOG					Instrument	var			
					[Fe/H]	σ	$v \sin i$	σ	MK	T_{eff}	σ	$\log g$	σ	[Fe/H]			σ	ξ_t	σ
11342410	5858	110	4.26	0.21	-0.07	0.22	1.8	0.6	G1V	—	—	—	—	—	—	—	—	FRESCO	
11396108	6330	169	3.97	0.22	-0.03	0.21	20.1	1.9	F6IV	—	—	—	—	—	—	—	—	FRESCO	
11414712	5731	93	4.16	0.21	0.02	0.21	2.3	0.9	G3V	5725	61	3.99	0.10	-0.02	0.05	1.27	0.01	NARVAL	⊙ (1)
11495120	4864	90	2.70	0.21	-0.09	0.21	2.9	0.5	G8III	—	—	—	—	—	—	—	—	FRESCO	⊙ (4)
11498538	6453	123	4.07	0.22	-0.01	0.21	33.2	1.3	F2V	—	—	—	—	—	—	—	—	ESPaDOnS	rot/act (6)
11551430	5649	141	4.01	0.22	-0.07	0.22	24.3	0.5	G5IV	—	—	—	—	—	—	—	—	FRESCO	
11559263	5633	175	4.02	0.26	0.08	0.21	5.3	0.6	G5III	5284	66	3.03	0.11	-0.02	0.06	0.77	0.03	HERMES	
11708170	6872	124	4.21	0.22	-0.04	0.21	32.9	2.3	F1V	—	—	—	—	—	—	—	—	ESPaDOnS	rot/act (6)
11709006	5852	104	4.38	0.21	0.01	0.21	10.2	0.2	G1.5V	6047	79	4.66	0.11	0.05	0.06	1.40	0.07	HERMES	
11717120	5155	104	3.76	0.27	-0.17	0.21	0.6	0.3	G9.5IV	5118	67	3.80	0.12	-0.27	0.06	0.89	0.04	FIES	⊙ (1)
...	5222	109	3.82	0.24	-0.17	0.21	1.1	0.4	G8IV	5137	65	3.87	0.12	-0.28	0.05	0.83	0.04	NARVAL	
11179629	—	—	—	—	—	—	—	—	—	—	—	—	—	—	—	—	—	ESPaDOnS	SB2 (15)
11754082	4742	94	2.77	0.23	-0.10	0.21	11.5	2.7	G9III	—	—	—	—	—	—	—	—	FRESCO	⊙ (4)
11772920	5209	121	4.34	0.23	-0.07	0.21	1.4	0.8	K1V	5341	80	4.44	0.13	-0.10	0.06	0.73	0.10	HERMES	⊙ (9)
12009504	6099	125	4.00	0.21	-0.14	0.22	5.9	0.7	F9IV-V	6267	71	4.37	0.11	-0.03	0.06	1.59	0.06	ESPaDOnS	⊙ (1)
12155015	3937	91	1.68	0.21	-0.16	0.21	2.8	0.9	K5III	—	—	—	—	—	—	—	—	ESPaDOnS	
12258514	5952	94	4.23	0.21	0.06	0.21	1.7	0.6	G0.5IV	6099	66	4.32	0.10	0.10	0.05	1.36	0.03	ESPaDOnS	⊙ (1)
12453925	6514	153	4.14	0.22	-0.02	0.21	75.2	2.9	F3V	—	—	—	—	—	—	—	—	ESPaDOnS	
12455203	4919	93	2.89	0.22	-0.02	0.21	2.3	0.3	G8III	5104	69	3.14	0.13	0.07	0.06	1.49	0.03	ESPaDOnS	⊙ (4)
12508433	5134	121	3.50	0.28	0.08	0.22	0.6	0.4	K0III-IV	5281	76	3.85	0.13	0.21	0.06	0.98	0.06	HERMES	⊙ (1)

* We use an asterisk to indicate stars listed by Bruntt et al. (2012) or Thygesen et al. (2012) who do not provide the information whether they used the ESPaDOnS or the NARVAL spectra in their analysis.

The equatorial coordinates and multi-colour magnitudes of the stars from this table are available at the Mikulski Archive for Space Telescopes (MAST) at http://archive.stsci.edu/kepler/kepler_fov/search.php

Literature:

(1) Huber et al. (2011); Chaplin et al. (2011), (2) Figulski et al. (2009), (3) Howell et al. (2012), (4) Hekker et al. (2011), (5) Stello et al. (2011), (6) Uytterhoeven et al. (2011), (7) Sergey (2007), (8) Šmelcer (2003), (9) Appourchaux et al. (2012), (10) <http://planetquest.jpl.nasa.gov/kepler/table>, (11) Fröhlich et al. (2012), (12) Frasca et al. (2011), (13) Verner et al. (2011), (14) Thygesen et al. (in preparation), (15) this paper.

Types of variability:

⊙: solar-like oscillations, δ Sct: δ Scuti-type pulsations, Mira: α Ceti-type pulsations, RS CVn: RS CVn-type variability, rot/act: star activity/rotational modulation, PER: strictly periodic with sinusoidal light-curves, APER: no well-pronounced periodicity, \wp : planet-hosting star, $\wp?$: candidate for a planet-hosting star, SB2: double-lined spectroscopic binary.